Biomedical Signal Processing and Control 82 (2023) 104589

Contents lists available at ScienceDirect

Biomedical Signal Processing and Control

journal homepage: www.elsevier.com/locate/bspc

A monitoring method of freezing of gait based on multimodal fusion

Bochen Li [a,b], Yan Li [a,b], Yining Sun [a], Xianjun Yang [a], Xu Zhou [a], Zhiming Yao [a,b,*]

[a] Hefei Institutes of Physical Science, Chinese Academy of Sciences, Hefei 230031, China
[b] University of Science and Technology of China, Hefei 230026, China

ARTICLE INFO

Keywords:
Inertial measurement unit
Force-sensitive insole
Monitoring of FOG
Multimodal fusion
Deep learning

ABSTRACT

Freezing of Gait (FOG) is an episodic lower extremity movement disorder that is highly susceptible to falls and carries a serious risk of disability. Monitoring of FOG can assist in the diagnosis and treatment of FOG. Providing appropriate gait guidance along with monitoring can help reduce the frequency and duration of freezing episodes. This study aims to improve the robustness of the monitoring model using multimodal fusion methods. The gait signals from 32 FOG patients are collected by the inertial measurement unit (IMU) and force-sensitive insole (FSI) simultaneously. A multimodal fused FOG monitoring model was constructed by using deep neural networks to extract complementary features from IMU and FSI signals respectively, and feature-level fusion of the two modalities by an adaptive weighting method. Experimental results show that the proposed multimodal fusion approach improves the F1 value by 0.029 in the FOG detection task compared to the unimodal model. In addition, to construct the pre-FOG dataset more accurately, an automatic labeling method of pre-FOG events based on the FOG index ratio is also proposed in this paper. Compared to directly labeling the data 2.5 s before the freezing episode as the pre-FOG event, the proposed labeling method obtained more samples and improved the freezing prediction accuracy by 1.4 %.

1. Introduction

Freezing of Gait (FOG) is an episodic lower extremity movement disorder that carries a serious risk of disability. During a freezing episode, the patients feel like they are “glued” to the floor, their gait is stagnant, and they cannot move. After a while, the patient may return to a normal gait. FOG events may appear suddenly at any time and place and last randomly for seconds to minutes [1,2]. This inadvertent onset of symptoms can easily cause patients to fall, severely impairing their mobility and posing a great threat to their lives [3]. At the same time, FOG is widely prevalent, with Parkinson’s disease, for example, affecting about 6.1 million people worldwide, of whom more than 63 % have symptoms of FOG [4,5]. However, until today the clinical detection of FOG has been based on scales and questionnaires, this kind of subjective assessment method relies on the experience of the physician, the description of the patients and their families, as well as the patient’s performance during the assessments. Due to the paroxysmal and random nature of FOG, doctors cannot accurately grasp the frequency and duration of freezing episodes, which causes great problems in the treatment and in-depth research of FOG [6]. FOG wearable monitoring aims to enhance the effect of intervention by using wearable devices to monitor FOG during daily activities in real time and give gait guidance when needed, which is important for clinical diagnosis and treatment of FOG.

1.1. The FOG detection method based on the inertial measurement unit

As a type of wearable device, the inertial measurement unit (IMU) has attracted much attention due to its small size, low power consumption, easy integration, and low price. In 2008, Moore et al. [7] performed a windowed Fourier analysis of the vertical acceleration signal at the patient’s ankle and found that the amplitude peaks of the power spectrum during freezing episodes were distributed between 3 and 8 Hz and within 3 Hz during normal walking, thus the ratio of the power in the “freezing” band (3–8 Hz) to the power in the “motion” band (0.5–3 Hz) was defined as the Freezing Index (FI). Since then, FI has gradually become a “benchmark” for assessing the severity of FOG, and various improvement methods based on FI have emerged [8–10]. However, such linear decision planes delineated by rule- or threshold-based methods are often difficult to cope with the complex and variable task of FOG monitoring. Subsequently, machine-learning-based methods were proposed and Mazilu et al. [11] used the methods for

* Corresponding author at: Hefei Institutes of Physical Science, Chinese Academy of Sciences, Hefei 230031, China.
E-mail address: zhmyao@iim.ac.cn (Z. Yao).

https://doi.org/10.1016/j.bspc.2023.104589
Received 17 May 2022; Received in revised form 20 December 2022; Accepted 9 January 2023
Available online 18 January 2023

the first time to build a FOG detection model and finally obtained a sensitivity of 0.663 and specificity of 0.954 under a model using the random forest as the classifier. Pepa et al. [12] designed features such as rhythm variation and energy derivative ratio and developed a fuzzy rule-based FOG detection algorithm that was able to reduce false-negative detection. Ashour et al. [13] used the infinite feature selection (IFS) technique to rank 135 features, eliminate redundant features, and achieve the highest individual accuracy of 0.944 for detection on the Daphnet dataset [14]. Nevertheless, due to the random start and end of FOG events, it is often difficult for hand-designed features to capture the inherent properties hidden in various time-series data, which leads to the lack of performance of traditional machine learning methods. El-Attar et al [15] implemented a patient-independent approach using the signals recorded by vertical acceleration sensors only. The discrete wavelet transform (DWT) was used to extract the main features inherent in the FOG detection of key motion metrics and then, the ability to evaluate the recognition of these features using support vector machines and artificial neural networks was compared. Using these two different machine learning techniques, FOG was detected with 87.50 % and 93.8 % accuracy, respectively. After that, they [16] considered three types of transformations and applied the features extracted from these transformations to machine learning methods such as artificial neural networks (ANN) to detect FOG. they integrated the features extracted from 1D DWT and FFT in the proposed hybrid system and achieved an accuracy of 96.28 % for PD detection established using the ANN.

The latest techniques use deep learning methods, which can be used to obtain more abstract feature representations by increasing the layers and depth of the network. Ashour et al, 2020 [17] used signals from accelerometers of wearable devices placed in different positions (on the hip, knee, and ankle) for the detection of FOG. They developed this model using a Long Short-Term Memory (LSTM) network, designed by considering patient dependency, and then compared this model to traditional machine learning techniques such as support vectors. They found that the LSTM network performed better, which achieved 83.38 % in terms of the average accuracy in comparison with the SVM which achieved 79.48 %.

In our previous studies [18], we constructed a novel FOG detection model SEC-ALSTM based on the characteristics of FOG, using IMU signals as input, deep learning techniques were used to design the neural network structure, compressed activation blocks, and attention mechanisms were introduced to enhance the feature representation capability of the network, and the accuracy of detection was significantly improved. However, since the IMU signals only capture gait kinematic parameters, the model still suffers from a lack of robustness in patient-independent generic model testing.

1.2. The FOG detection method based on force-sensitive insole

Force-sensitive insole (FSI) captures both gait kinetic and gait kinematic parameters, making it ideal for monitoring FOG at home. However, international research on FOG monitoring based on FSI is still in its infancy. Howcroft et al. [19] performed fall detection work for the elderly based on an array of FSIs (F-Scan 3000E, Tekscan) using Relief-F. Shalin et al. [20] also used F-Scan to obtain foot pressure distribution signals, and they stitched the left and right foot pressure distribution data into a 60×42 matrix, and extracted features such as Centre of Pressure (COP) location, COP velocity, COP acceleration and GRF from the matrix, and then designed a FOG detection model with a 2-layer LSTM network. Thus, preliminary studies using FSI signals for gait analysis and related detection tasks have shown promising applications, and FSIs are expected to be a key to improve the performance of FOG monitoring. The information between the FSI signals and the IMU signals are complementary, thus it can be speculated that combining the FSI distribution signals with the IMU signals may be an effective way to improve the robustness of the FOG monitoring model.

1.3. The prediction method of FOG

In addition, it has been shown that freezing episodes are a “sequential effect” of progressive gait deterioration [21,22]. Clinical studies have observed impaired gait cycles such as increased cadence, decreased rhythm, increased left–right asymmetry, and gait disturbances, before the FOG episodes [23]. These characteristics offer the possibility to predict FOG, and if cues can be provided before the onset of freezing, it may be possible to break the “sequence effect” of gait deterioration and effectively prevent the occurrence of FOG. However, the transition from normal to FOG is subtle and often not visually discernible, so the best pre-FOG segment is often difficult to determine [24]. Most of the existing studies have directly labeled the fixed time window before the freezing episode as pre-FOG [25–27], a simple but poorly accurate method. Since the duration of pre-FOG varies both within and between patients. It is difficult to convincingly label the pre-FOG events directly using a fixed length of time. Some investigators have also automatically determined the duration of the pre-FOG based on the progressively worsening gait characteristics before FOG. For example, Zhang et al. [28] segmented the gait signal according to the gait period and labeled the pre-FOG in walking based on the accelerated cadence before the FOG episode. Nevertheless, this kind of method is also limited, because the segmentation of the gait period sometimes does not work when FOG is about to come, as the gait patterns of the patient are impaired and the periodic features become more and more confusing. How to identify abnormal signals before freezing episodes to mark pre-FOG, and how to extract key features from signals before freezing episodes to improve the accuracy of FOG prediction models are worth further study.

1.4. Contributions

In order to further improve the accuracy of FOG wearable monitoring, this paper adopts the strategy of multi-sensor fusion to carry out the detection and prediction of FOG respectively. The main work of this paper includes the following two points:

(1) To enhance the robustness and accuracy of the FOG monitoring model, this paper uses a multimodal fusion approach to combine IMU signals and FSI signals for FOG monitoring. Firstly, the IMU signals feature expression method was designed based on the SEC-ALSTM model proposed in our previous study; then the plantar pressure partitioning was performed according to the characteristics of the plantar pressure signal, and the plantar pressure distribution feature map was constructed, and a 2D convolutional neural network was used for feature representation; finally, the adaptive weighting method was used to fuse the IMU signals and the feature vector of the FSI signals to construct a multimodal fused FOG monitoring model.

(2) To improve the marking accuracy of pre-FOG, a pre-FOG automatic marking method is proposed based on the FI. The results show that the quality of the marked data obtained by this method is improved, and the multimodal fusion model proposed in this paper is used to perform the FOG prediction task with improved prediction.

The rest of the paper is organized as follows. Section 2 describes the data acquisition process, data preprocessing, and the procedure for the construction of the multimodal fusion model. Section 3 describes the situation of the acquired dataset and the performance of the FOG detection model and the prediction model. Section 4 is a discussion and analysis of the model detection and prediction results, as well as several limitations of this study. Finally, in Section 5, the work and contributions of this study are summarized.

2. Materials and methods

2.1. Data acquisition

2.1.1. Subject screening criteria

The subjects in this study were all patients with FOG, whose inclusion criteria were a FOG-Q questionnaire score greater than 6 and at least one FOG event experienced in the past week. Before the subjects are assessed with the questionnaire, a FOG video will be shown to help them establish a correct perception of FOG symptoms. The participants were excluded according to the following criteria: (a) Suffering from gait-limiting syndromes, such as orthopedic conditions; (b) Suffering from a serious mental illness, such as major depressive disorder. (c) Inability to complete the required movements or to cooperate well with the doctor to complete the test.

To ensure the validity of data collection, all experiments were performed after approval by the hospital's ethical research committee and with the cooperation of physicians. Before the experiments, basic information of participants was recorded and all participants underwent a clinical assessment using the UPDRS and the FOG-Q questionnaire. The experimental procedure strictly followed the Declaration of Helsinki and was approved by the Academic Ethics Committee of the University of Science and Technology of China, and subjects were informed of the purpose of the experiment as well as potential risks before proceeding, and then signed an informed consent form.

2.1.2. Device wearing scheme

As shown in Fig. 1, we use two IMUs and a pair of FSIs to obtain the patient's gait signal simultaneously. The IMUs (LMPS-B2, a 9-axis miniature wireless transmission posture sensor with an integrated 3-axis accelerometer, 3-axis gyroscope, and 3-axis magnetometer manufactured by Guangzhou Alubi Electronic Technology Co.) were worn on the lateral side of the patient's right and left ankles, respectively. F-Scan pressure insoles (Tekscan, Boston, MA) are used for foot pressure data recording. F-Scan insoles are thin (<1 mm) plastic film sheets with 3.9 pressure sensing cells per cm^2 and can be trimmed to fit every participant to ensure accurate data acquisition. The data is collected while the video is recorded using a wide-angle camera for category tagging of gait signals.

2.1.3. Experimental procedure

As shown in Fig. 2, subjects were asked to complete two walking test tasks: (1) Free walking. Subjects were allowed to walk normally as they wished in a given experimental site, which was designed to simulate the walking patterns of patients in their daily lives, making the data collected in the study more consistent with the patients' daily walking patterns. (2) Prescribed route walking. Subjects were asked to follow a pre-designed route, which could include a variety of FOG-inducing scenarios such as starting, stopping, 90°, 180°, and 360° turning, crossing narrow passages, dual tasks, and crossing obstacles, where the dual tasks were designed to perform additional tasks while walking, such as walking with a glass of water and asking them to spill the less water possible, and answering questions while walking (e.g., personal preferences, addition, and subtraction within 100, etc.). The purpose of the prescribed route walking is to induce FOG events during the walking test. Considering that different subjects are sensitive to different freezing-induced scenarios, the experiment was customized for each subject with the cooperation of a physician. IMU signals and FSI signals were collected simultaneously during the experiment.

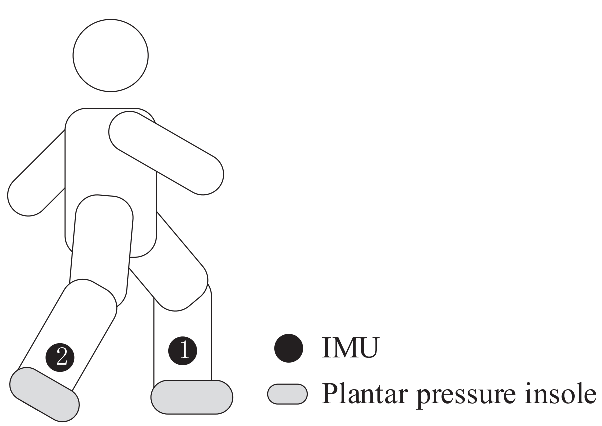

Fig. 1. Diagram of device wearing solution. Two IMUs are worn on each side of the patient's shank (just above the ankle) by elastic straps, and the FSIs are cut to the suitable size and placed directly in the patient's shoes.

2.2. Data preprocessing

Before fusing the data, we need to pre-process it, which includes labeling the FOG based on the video recording, data filtering, plantar pressure signal partitioning, sample segmentation, etc.

2.2.1. FOG labeling

The acquired data were marked by video playback for FOG onset time, and the video was played back by the Avidemux video editor. FOG events that occurred during the experiment were marked by three specialized physicians using a voting process.

2.2.2. Outlier processing

Although the data acquisition software of LMPS-B2 comes with a Kalman filter for noise reduction of the original data, there may still be outliers in the original IMU signals, and these outliers can seriously affect the energy distribution of the IMU signals. Since the frequency histogram of the IMU signal approximately follows the Gaussian distribution, the "4σ Criterion" can be used for outlier detection. Specifically, the sample data falling outside the 4σ interval are considered outliers. In previous studies, outliers were often replaced by the median [18], but this method may introduce a strong bias affecting skewness and kurtosis. For this reason, we adopt two outlier processing methods, median replacement, and direct removal, then compare the performance of the two methods.

The plantar pressure distribution data is a time series pressure distribution matrix. The single frame of plantar pressure distribution data is a two-dimensional matrix of size 60×21, containing a total of 955 valid pressure points, with each pressure point taking values in the range of 0–255, and the left and right foot plantar pressure distribution data are stitched together as shown in Fig. 3. The raw plantar pressure data contained outliers, which could be derived from current noise, environmental noise, and anomalous values generated by the deformation of the insole during walking [29]. Here, a plantar pressure signals filtering method that we proposed in previous research was used [30]. First, go through each valid point in the single-frame pressure insole data matrix and calculate the number n of valid points in the 8 neighborhoods of each point. If n is less than the set threshold, the point is marked as an outlier, assuming the point is noted as $f_t(\mathrm{i},\mathrm{j})$, with i denoting the row and j denoting the column. Four frames of data before and after the frame where $f_t(\mathrm{i},\mathrm{j})$ is located are selected, as shown in Fig. 4, and the values in row i and column j of these data are put into $\mathrm{F}_t(i,j)$, $F_t(\mathrm{i},\mathrm{j}) = [f_{t-4}(\mathrm{i},\mathrm{j}), \cdots, f_{t+4}(\mathrm{i},\mathrm{j})]$, if the number of valid points in $F_t(i,j)$ is less than the set threshold, then $f_t(\mathrm{i},\mathrm{j})$ will be replaced with invalid points.

2.2.3. Plantar pressure zone

The plantar pressure distribution signal contains abundant information on gait dynamics, but at the same time the data scale is huge, and if the original data is directly used as the input signal for feature extraction or FOG detection, it will inevitably bring a high number of network parameters and floating points operations, which in turn makes

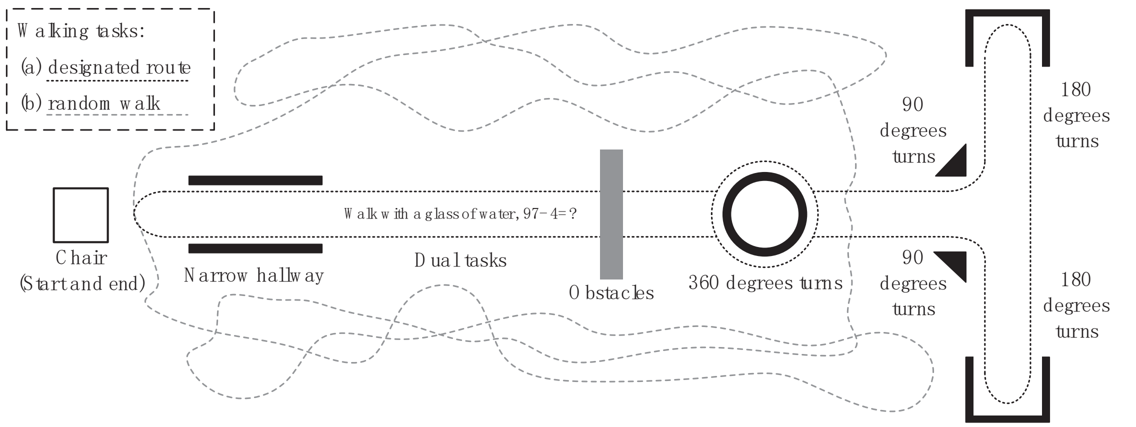

Fig. 2. Walking path planning sketch.

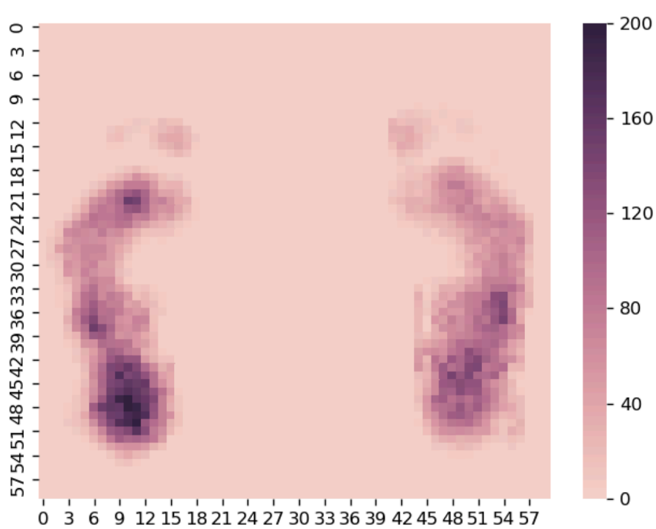

Fig. 3. Splicing of plantar pressure data of both feet. The matrix size of a single insole is 60 * 21, and the matrices of two insoles are stitched together to form a 60 * 60 matrix, with a 60 * 18 zero matrix filling in between.

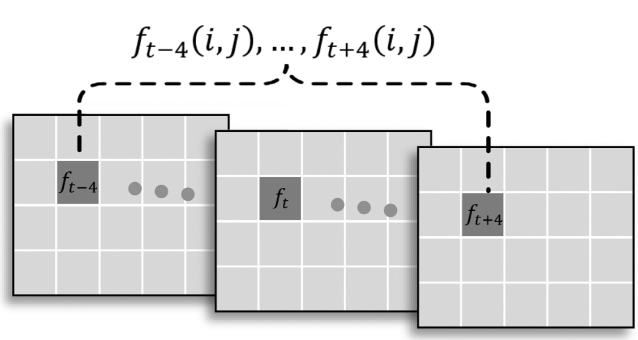

Fig. 4. Instructions for removing outliers along the time dimension.

the model more complicated. Clinically, a partitioning approach is usually used to process plantar pressure distribution data [31–33], as shown in Fig. 5, where we divide the plantar pressure matrix into 10 regions corresponding to the anatomical structure of the foot [30] and use the average pressure in each region to represent the abstract features of the plantar pressure distribution in that region.

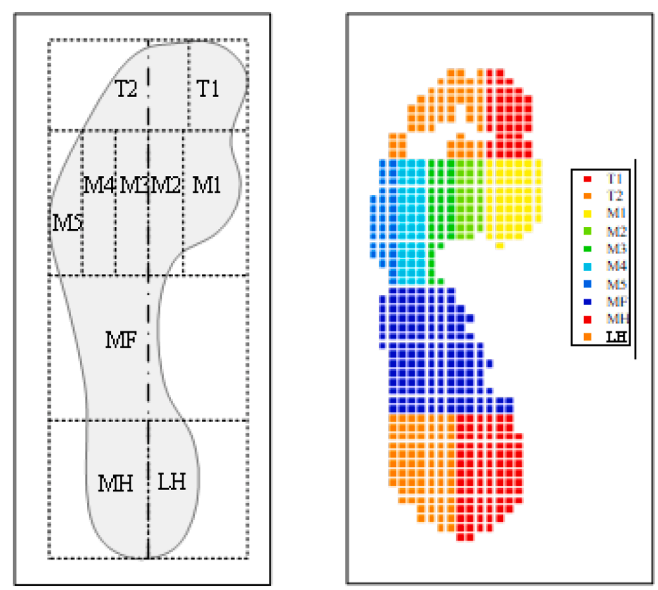

Fig. 5. Plantar pressure distribution. Where T1 and T2 are the regions of the toes, M1-M5 are the regions of the sole, MF is the region of the arch, and MH and LH are the regions of the heel.

2.2.4. Sample segmentation

The IMU and plantar pressure distribution signals were segmented using a sliding window, and since the physician's marker had been added to each frame of data, i.e., each frame of data had a gait label, the gait label that appeared most times in each of the samples segmented by the window was used as the label for that window sample.

2.3. Freezing gait detection model based on multimodal fusion

2.3.1. Characteristic expression of IMU signal

In our previous study, we construct a novel FOG monitoring model based on the characteristics of IMU signals, which consists of a deep convolutional neural network containing SE blocks and an attention-enhanced LSTM network (ALSTM), which we call SEC-ALSTM [18]. The specific structure of the SEC-ALSTM model is shown in Fig. 6. In this paper, we use the SEC-ALSTM network with the Fully Connected layer removed as a feature representation network for IMU signals and construct an IMU feature vector of length 128.

2.3.2. Characteristic expression of FSI signal

Plantar pressure during normal walking in humans shows cyclic

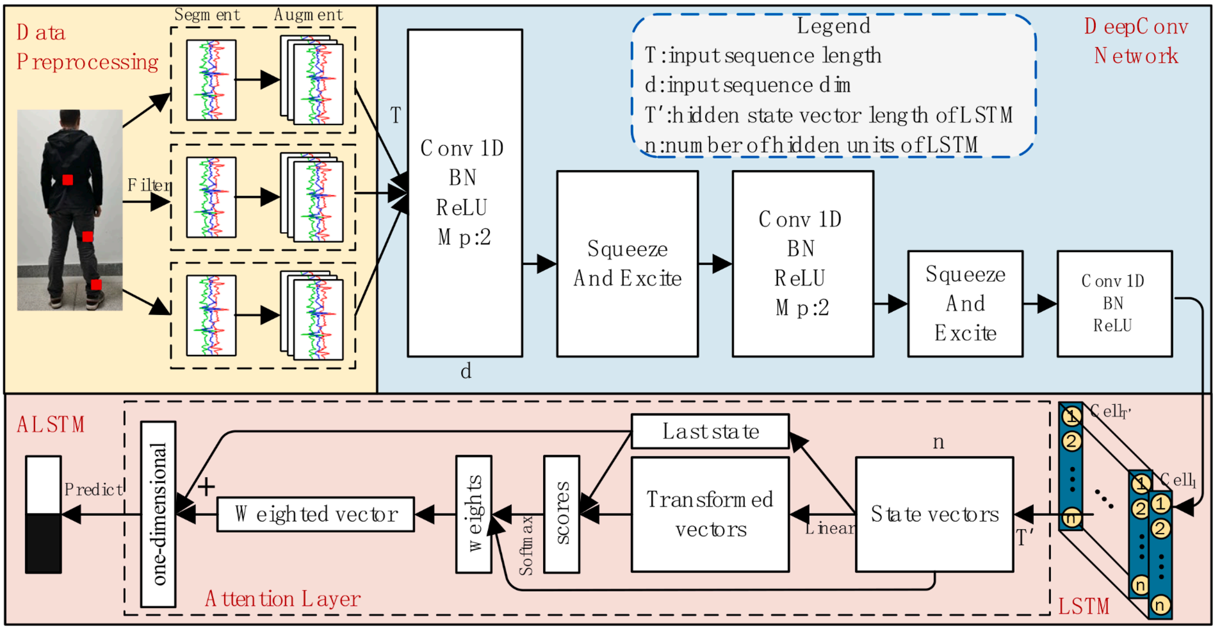

Fig. 6. The architecture of SEC-ALSTM. Conv 1D is a one-dimensional convolutional layer, LSTM is a long short-term memory recurrent neural network, squeeze-and-excitation block is used to converge the global information of each channel of the network. "Bn", "ReLU" and "MP" are the abbreviations of "Batch normalization", "Rectified Linear Unit", and "Max pooling layer" respectively. T is the length of data instance in the temporal dimension, d is the dimension, T′ is the hidden state vector length of LSTM, and n is the number of hidden units of LSTM.

changes. By dividing the plantar pressure distribution data into ten regions according to the anatomical definition, and then analyzing the cyclic characteristics of foot pressure during walking, as shown in Fig. 7, it can be seen that the force areas always cycle between the regions in a fixed order.

Therefore, we partitioned all frames of data within a 4-second sliding window into ten regions using the foot pressure partitioning algorithm described in the previous section and then stitched the average pressure of all partitions in a fixed order of T1-T2-M1-M2-M3-M4-M5-MF-MH-LH, and finally stitched the partitioned average pressure signals of both feet in the order from left to right to obtain the combined signals as shown in Fig. 8, which is the input feature map of the mixed stream.

Based on the characteristics of the plantar pressure signal feature map, we designed the feature representation network, called Insole-ConvNet, using deep learning techniques. As shown in Fig. 9, the designed Insole-ConvNet is based on a 2D convolutional structure, and the main body of the network consists of five convolutional modules, each of which contains a convolutional layer, a Batch Normalization (BN) layer [34], and an activation layer with ReLU as the activation function. The convolutional layer has the characteristics of local connection and weight sharing, which can reduce the scale of network parameters and accelerate the convergence of the network; the batch normalization layer can make the output data of convolution distributed in the sensitive interval of activation function to prevent "gradient dispersion", accelerate the convergence and avoid gradient disappearance or explosion; ReLU activation can make the output of some neurons zero, which makes the network structure more sparse and reduces the interdependence between network parameters, and effectively alleviates the overfitting problem of convolutional neural network. The size and step length of the convolution kernel is designed according to the feature map size. In addition, a Max Pooling layer is added between the first four convolution modules to compress the number of model parameters and prevent overfitting. The number of output feature map channels of the last convolution module is 128, and a feature vector of length 128 is obtained by Global Average Pooling (GAP). To verify the effectiveness of the Insole-ConvNet network, a Fully Connected (FC) layer is added after the GAP layer of Insole ConvNet, and a softmax activation function is used for FOG detection.

2.3.3. *Feature-level integration of IMU and FSI*

As shown in Fig. 10, feature-level fusion was used to construct a multimodal fusion freeze gait monitoring model. However, since the two modalities, plantar pressure distribution signal and IMU signal, contribute differently to the freezing gait detection task, and there may be redundant or complementary relationships between the two features, directly concatenating the feature vectors is not the best strategy. Therefore, feature fusion is placed in a deep neural network framework, which performs an adaptive fusion of feature parameters by automatically masking redundant features and highlighting complementary features through network training.

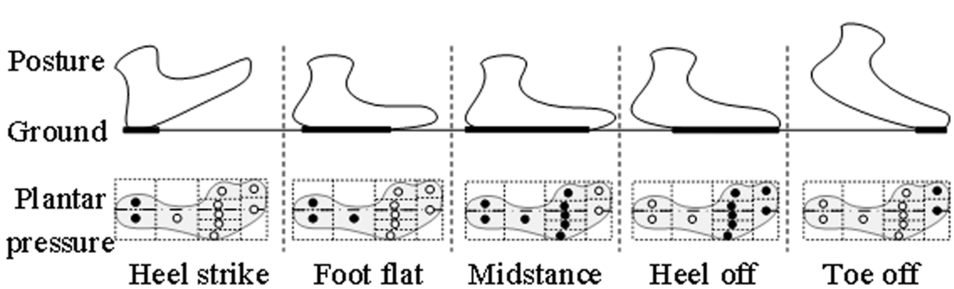

Fig. 7. Periodic changes in plantar pressure distribution during normal walking. The solid black dots (●) represent the main distribution areas of pressure.

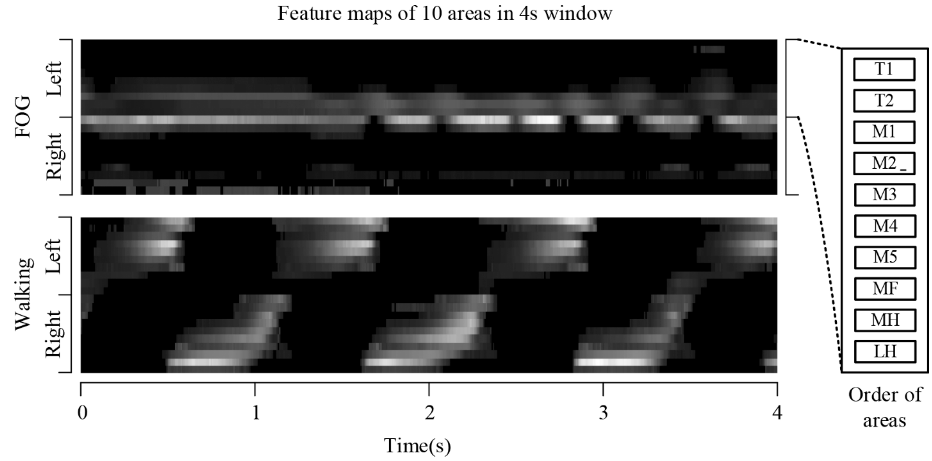

Fig. 8. Comparison of mixed flow characteristics during normal walking and freezing. The bottom half of the figure is a time series plot formed by partitioning and stitching the pressure distribution data of a normal Participant, while the top half is a time series plot of a FOG patients.

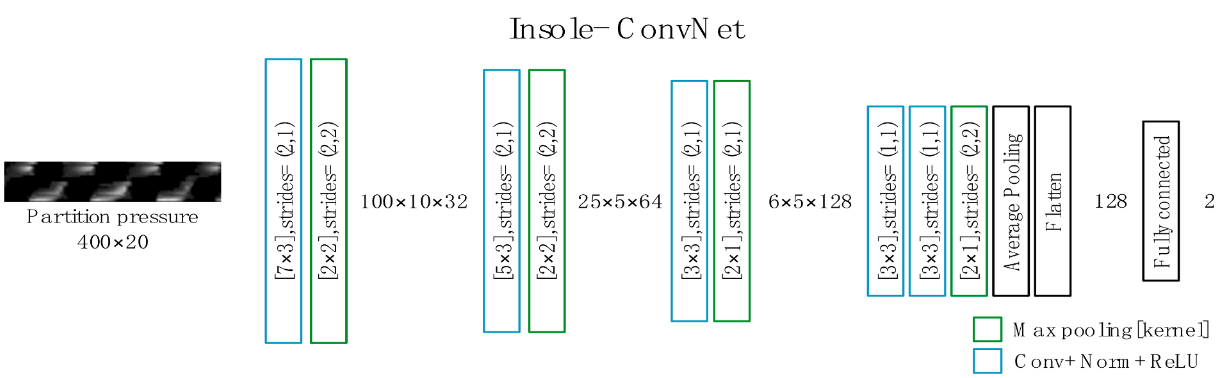

Fig. 9. Feature representation network of FSI data.

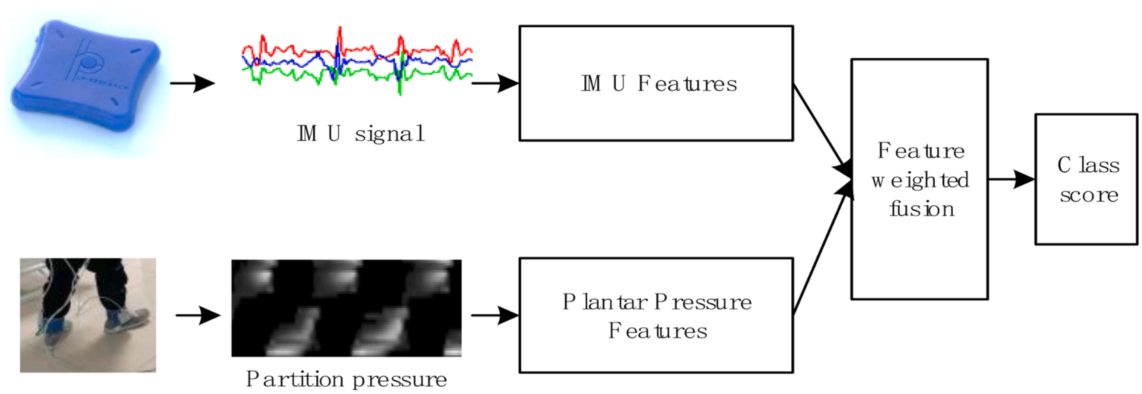

Fig. 10. Processing flow of IMU and FSI signals.

The computation process of adaptive weighted fusion features is illustrated in Fig. 11, where we assign a weight to each feature parameter to indicate how important that feature parameter is for the FOG detection task. The size of the weights can be learned automatically by neural network training. Feature parameters are automatically assigned larger weights if they reduce model loss and vice versa. Suppose $\boldsymbol{F_I}$ is the inertial feature vector output by the SEC-ALSTM model after removing the last layer, $\boldsymbol{F_P}$ is the feature vector output by the Insole-ConvNet network after removing the Fully Connected Layer, and $\boldsymbol{F}$ is the feature vector after concatenating the two feature vectors. Then $\boldsymbol{F}$ can be obtained as:

$$F = concat(\boldsymbol{F}_I, \boldsymbol{F}_P) = \begin{bmatrix} \boldsymbol{F}_I \\ \boldsymbol{F}_P \end{bmatrix} \quad (1)$$

Next, the weights are assigned to the feature vectors $\boldsymbol{F}$ after the concatenation to obtain the fused feature vector $\boldsymbol{F_F}$, which is calculated as follows:

$$\boldsymbol{F}_F = \alpha F = \begin{bmatrix} \boldsymbol{\alpha}_I \boldsymbol{F}_I \\ \boldsymbol{\alpha}_P \boldsymbol{F}_P \end{bmatrix} \quad (2)$$

Where $\boldsymbol{\alpha}$, $\boldsymbol{\alpha}_I$, and $\boldsymbol{\alpha}_P$ denote the weight vectors. After obtaining the fused feature vector $\boldsymbol{F_F}$, the category score P is calculated as:

$$P = softmax(\boldsymbol{W}\boldsymbol{F}_F + \boldsymbol{b}) \quad (3)$$

Where $\boldsymbol{W} \in \mathbb{R}^{C*F}$ and $\boldsymbol{b} \in \mathbb{R}^{C}$ are the learnable weight matrix and bias

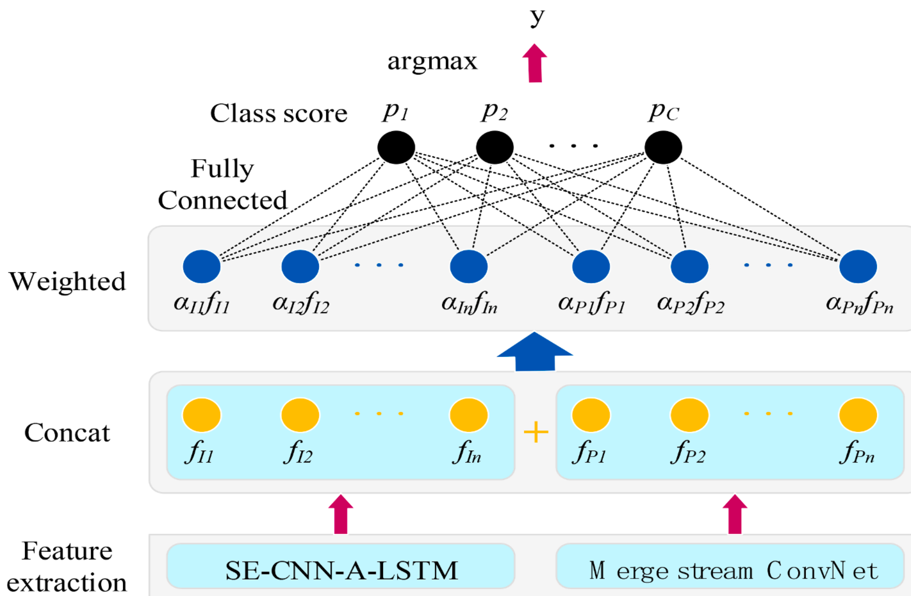

Fig. 11. Adaptive weighting-based feature fusion.

vector, respectively. C is the number of classification categories and F is the dimensionality of the fused feature vector. *softmax* function is defined as:

$$softmax(z_j) = \frac{e^{z_j}}{\sum_{i=1}^{C} e^{z_i}}, j = 1, 2, \cdots, C. \quad (4)$$

Finally, the final predicted categories are calculated as:

$$y = argmax(\boldsymbol{P}) \quad (5)$$

The net loss in the feature fusion model is calculated by the cross-entropy loss function as:

$$loss = \frac{1}{N}\sum_i loss_i = -\frac{1}{N}\sum_i \sum_c^C y_{ic} \log(p_{ic}) \quad (6)$$

where N is the total number of samples and p_{ic} denotes the probability that sample i belongs to category c. y_{ic} is a symbolic function and can be expressed as follows:

$$y_{ic} = \begin{cases} 0, \text{The true category of sample i is c} \\ 1, \text{The true category of sample i is not c} \end{cases} \quad (7)$$

Suppose f_i denotes the i th characteristic parameter of $\boldsymbol{F}$, α_i denotes the weight of the characteristic parameter f_i, and the weighted characteristic parameter is $\alpha_i f_i$ in error backpropagation with the following equation:

$$\frac{\partial loss}{\partial f_i} = \alpha_i \frac{\partial loss}{\partial(\alpha_i f_i)} \quad (8)$$

2.3.4. Pre-FOG marking method

Real-time detection of FOG certainly helps physicians to have a more complete picture of the condition, but it does not reduce the number of freezing episodes. For patients, predicting FOG events before they occur allows interventions to improve gait patterns and thus inhibit the onset of FOG, which is of great importance in preventing falls and improving the quality of life of patients. Previous studies have shown that FOG occurs as a gradual deterioration of gait, characterized by a gradual reduction in stride length and increased energy of the “freezing” band [23]. Thus, we improved on the previous studies by using the FI [7], which is widely recognized by researchers, for the pre-FOG category labeling task. The FI can be calculated as:

$$FI = \frac{Powerin\ 'freeze'\ band}{Powerin\ 'locomotor'\ band} \quad (9)$$

where the frequency range of the 'freeze' band is 3 Hz–8 Hz and the frequency range of the 'locomotor' band is 0.5 Hz–3 Hz.

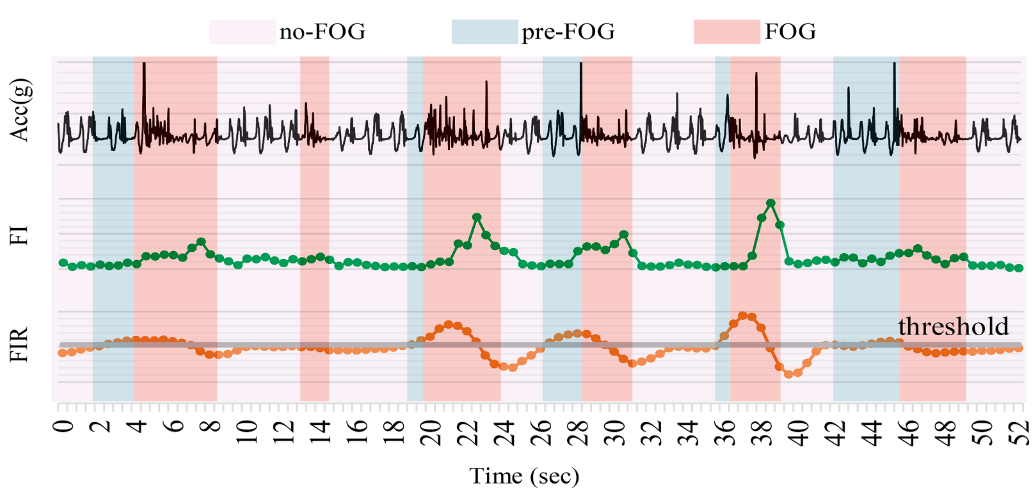

Fig. 12. Freeze index and freeze index ratio calculated from a segment of the accelerometer signal. The left border of the light blue vertical bar is the location of the start of pre-FOG, which is determined by where the red line breaks the threshold. (For interpretation of the references to colour in this figure legend, the reader is referred to the web version of this article.)

As shown in Fig. 12, before the onset of FOG, the FI gradually increases until it reaches its maximum during the freezing episode, which is the basis for our labeling of the pre-FOG category. First, the inflection point of the rising FI curve needs to be found as the starting point of the pre-FOG phase. For this purpose, we define the Freeze Index Ratio (FIR) and use the point in the signal where the FIR (the red line in Fig. 12) first rises above a preset threshold as the inflection point of the rising FI Curve. In this paper, we use the "trial and error method" to find the optimal threshold, and use the optimal value as the FIR threshold. Similarly, we add windows to the signals, and the FIR for the *i*th window is defined as follows:

$$FIR(i) = \frac{\sum_{j=i+1}^{i+n} FI(j)}{\sum_{j=i-n}^{i-1} FI(j)} \quad (10)$$

where $FI(j)$ denotes the FI of the j th window. Here, we choose a sliding window length of 2 s, a step length of 0.5 s, and n is taken as 4. Based on the experience of previous studies [25–27], we believe that the maximum period from the beginning of the freezing signs to the start of FOG will not exceed 6 s. Therefore, the 6 s before each freeze step onset is considered as the period in which pre-FOG may appear, and then the FIR of the signal is calculated during this period, and the period from the moment when the FIR is first above a preset threshold to the start of the FOG is labeled as pre-FOG.

3. Results

3.1. Description of the dataset

Participants were recruited from three hospitals: the Affiliated Hospital of the Institute of Neurology, Anhui University of Traditional Chinese Medicine; the First Affiliated Hospital of the University of Science and Technology of China, and the Second Affiliated Hospital of Anhui Medical University. As shown in Table 1, gait data were collected from 32 patients (21 males and 11 females) with FOG, with a total data duration of 526 min, during which there were 770 FOG events, as shown in Fig. 13. The duration of freezing events ranged from 1 to 264 s, with more than 50 % of freezing events lasting <4 s, and the vast majority of freezing events (91.7 %) lasted <20 s.

A sliding window was used to construct the sample set with a window length of 4 s and a step size of 0.5 s, and a total of 16,524 cases were obtained.

3.2. Experimental setup

The leave-one-out method cross-validation was used to evaluate the model performance by randomly dividing all samples into five groups according to subjects, selecting one of the groups as the test set and using the rest of the samples for training and validation, repeating the procedure until all subjects' samples were tested, and taking the average of the five cross-validations as the final evaluation result. The model performance was measured using the metrics of sensitivity, specificity, accuracy, AUC, EER, and F1 value, where the F1 value was calculated as follows:

Table 1
Basic information of the participants.

Group	FOG
Number of Patients	32
Age (Years)	53.3 ± 19.7
Gender	21M, 11F
UPDRS III-item FOG	2.1 ± 1.2
FOG-Q	13.9 ± 6.4
Sampling Rate (Hz)	100
Test duration (min)	526
Number of Freeze Events	770

$$F1 = \frac{2 * Precision * Recall}{Precision + Recall} \quad (11)$$

where Precision and Recall denote accuracy and recall, respectively, and the FOG category is considered as true.

Models were built based on PyCharm 2019 and Tensorflow 1.13.1 deep learning library and trained based on the minimized cross-entropy loss function. The computer hardware platform used for the experiments was configured with an Intel(R) Core(TM) i5-9400 CPU@2.90 GHz processor, an Nvidia GeForce RTX 2060 6 GB GPU graphics card, and 8 GB dynamic memory.

3.3. Performance of multimodal fusion FOG detection model

3.3.1. Comparison of detection performance of different models

To verify the effectiveness of the proposed multimodal fusion method, we compare the experimental results of four models: IMU-Model denotes the unimodal SEC-ALSTM model, Insole-Model denotes the unimodal Insole-ConvNet model, Feature-Fusion-Concat denotes the fusion model with the direct serial association of features, and Feature-Fusion-Weighted denotes the fusion model with feature adaptive weighting. Model training is performed based on minimizing the cross-entropy loss function. The experimental results are shown in Table 2, and the corresponding ROC curves are shown in Fig. 14.

As it can be seen in Table 2, the Feature-Fusion-Weighted model has the best overall performance with a sensitivity of 0.924, a specificity of 0.983, an accuracy of 96.3 %, and an F1 value of 0.943. The F1 value of the Feature-Fusion-Weighted model has improved by 0.008 compared to the Feature-Fusion-Concat model and compared to the unimodal IMU-Model model and Insole-Model model by 0.033 and 0.029, respectively. All evaluation metrics of the two feature fusion models outperformed the two unimodal models, with the F1 value improving by more than 0.02. In addition, the ROC curve shows that the AUC value of the Feature-Fusion-Weighted model is 0.992, which is not much different from that of the Feature-Fusion-Concat model, but the EER value is reduced by 0.6 %. The EER values of both feature-fusion models decreased by more than 1 % relative to the unimodal model.

Further, to determine whether the results obtained by the proposed model are statistically different from those obtained by other methods, Wilcoxon signed-rank tests were performed between the accuracies, and F1-scores obtained by these models. In these tests, p-values were calculated after performing 6 experiments. If the p-value was less than the 0.05 significance level, there was a significant difference between these methods. Table 3 tabulates the average p-values of the proposed model when compared with other models. Obviously, the proposed Feature-Fusion-Weighted model is statistically different from other counterparts with a 5 % significance level in terms of accuracy and F1-score performance.

3.3.2. Results of different outlier processing methods

Considering that median replacement may introduce an important deviation that affects skewness and kurtosis, we compared the performance of two IMU signal outlier data processing methods, namely median replacement and direct removal, for FOG detection. As shown in Table 4, there is no significant difference between the results obtained by the two outlier processing methods based on IMU Model. The FOG detection accuracy is higher than 94 %, and the F1-Score is higher than 0.910. This proves that removing outliers directly will not reduce the performance of FOG detection. The reason why the detection performance of the model using the median replacement method does not decline significantly may be that there are fewer outliers in the experimental samples, so there is no significant impact on the overall data distribution. However, we need to beware of the potential threats associated with the direct use of median substitution in certain scenarios. In addition, the results of this experiment show that in the actual scenario of FOG detection, an occasional small amount of data packet loss may have less impact on the results of detection, which is conducive

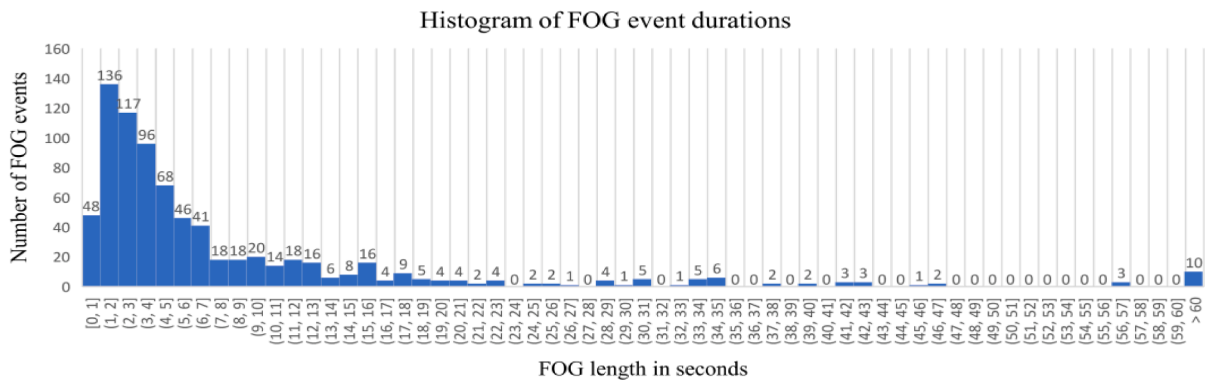

Fig. 13. IIM-FOG-IMU-Insole Dataset Freezing Event Duration Distribution Histogram.

Table 2
Detection results of different models.

Model	TPR	TNR	NPV	PPV	ACC	F1-Score
IMU-Model	0.877	0.975	0.946	0.941	94.3 %	0.910
Insole-Model	0.911	0.959	0.917	0.956	94.3 %	0.914
Feature-Fusion-Concat	0.916	0.978	0.954	0.960	95.8 %	0.935
Feature-Fusion-Weighted	0.924	0.983	0.963	0.963	96.3 %	0.943

to the application of FOG detection equipment using Bluetooth communication.

3.3.3. *Results of the separate study for genders*

Considering the sexual dimorphism in the locomotion process (differences in weight, limb length, bone structure, etc.), a separate study was conducted for both. Two datasets were constructed using the signals of male and female subjects respectively, and the multimodal fusion FOG detection model was trained and tested. The experimental results are shown in Table 5. The F1 values obtained from the male samples, the female samples, and the mixture of male and female samples were similar, indicating that the detection effect of the proposed model was not affected by gender and had high FOG detection accuracy for both male and female subjects. The F1 values of the Female group were slightly lower than those of the Male group, but their Specificity and Accuracy values were higher. Analysis of the raw data showed that the FOG events in the Female group occurred more frequently and the data were more balanced, while the ratio of FOG : noFOG in the Male group was 670:5302, which had a serious imbalance, leading to more difficulty in model training and the model tended to identify the noFOG samples more. This is also the reason why the Accuracy value is higher in the Male group but the F1 value is slightly lower. In addition, the number of FOG samples in the Male group is less than one thousand, which may lead to insufficient training of the model and thus reduce the overall

Table 3
Summary of Wilcoxon's signed ranks tests. The 5% level of significance is selected.

Model	Feature-Fusion-Weighted			
	ACC		F1-Score	
	p-value	Significant?	p-value	Significant?
IMU-Model	<0.01	Yes	<0.01	Yes
Insole-Model	<0.01	Yes	<0.01	Yes
Feature-Fusion-Concat	<0.01	Yes	<0.01	Yes

Table 4
Detection results of different outlier processing methods.

Method	TPR	TNR	PPV	NPV	ACC	F1-Score
Median replacement	0.877	0.975	0.946	0.941	94.3 %	0.910
Direct removal	0.894	0.972	0.949	0.940	94.6 %	0.917

Table 5
Detection results by gender.

Modal	TPR	TNR	PPV	NPV	Accuracy (%)	F1-Score
Male	0.919	0.970	0.965	0.913	94.6	0.941
Female	0.922	0.992	0.935	0.990	98.4	0.929
All patients	0.924	0.983	0.963	0.963	96.3	0.943

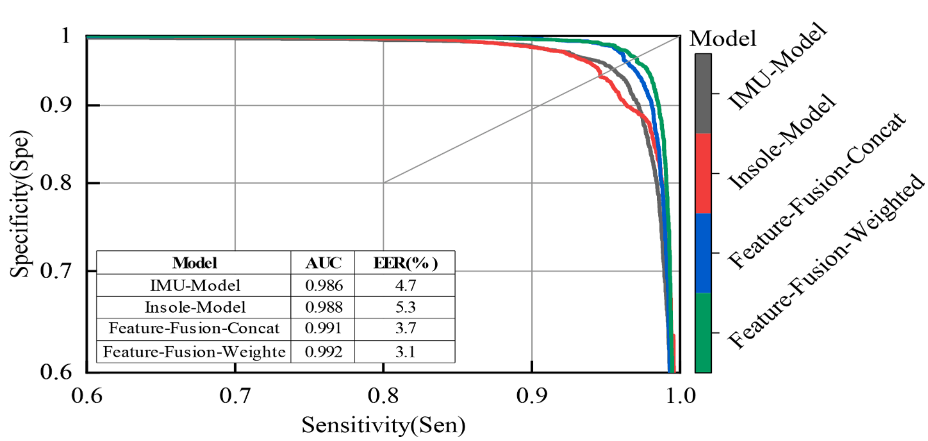

Fig. 14. ROC curves of the detection results of different models.

accuracy of the model.

3.4. Performance of FOG prediction models with multimodal fusion

The pre-FOG events labeling was performed using the pre-FOG labeling method described in the previous section based on the resultant acceleration signal at the ankle on the side of the patient with more severe gait impairment. Fig. 12 shows an example of pre-FOG events' labeling, and it can be seen that the proposed method based on the FIR can well capture the inflection point of the rising FI and realize the automatic labeling of pre-FOG.

To further validate the effect of the FIR method, the data set was relabeled using the fixed time length method, the data window with a fixed period before the freezing episode was re-labeled as the pre-FOG category, and the time lengths were chosen as 1.5 s, 2.5 s, 3.5 s, 4.5 s, and 5.5 s. A sliding window was used to construct the sample set, and to reduce the time delay of FOG prediction, the sliding window length was set to 1 s with a step length of 0.2 s. Data containing both events were not included in the sample set. The sample distribution of the re-labeled dataset is shown in Table 6. It should be noted that the number of pre-FOG samples is much less than the number of no-FOG samples, and directly training the unevenly distributed dataset would result in skewed class problems, so the no-FOG samples are randomly downsampled to ensure the robustness of the training model.

Using the previously proposed Feature-Fusion-Weighted multimodal fusion model for FOG prediction, Table 7 demonstrates the FOG prediction results using FIR and fixed time length for pre-FOG category labeling, respectively. It can be seen that the best result is achieved by the method using a fixed duration of 1.5 s with an F1 value of 0.786 followed by the method using FIR with an F1 value of 0.722. The prediction effect of marking using a fixed duration of 2.5 s is similar to that of the method using FIR with an F1 value of 0.721. However, the method using the FIR yields 3657 cases of pre-FOG samples, which were significantly more than the 2700 cases obtained with a fixed time length of 2.5 s. The mean duration of pre-FOG obtained using the FIR method was 3.22 s. In addition, the fixed duration method significantly decreased the prediction effect as the duration increased. When the set pre-FOG duration exceeds (equals to) 3.5 s, the F1 value is lower than 0.7 and the sensitivity is<0.6. Fig. 15 shows the ROC curves of the prediction results using different pre-FOG labeling methods. Among them, the AUC value using the FIR labeling method is 0.817, which is second only to the labeling method using a fixed duration of 1.5 s.

4. Discussion

The plantar pressure distribution signals contain abundant information on gait dynamics and the IMU signals contain abundant information on gait kinematics. We used an adaptive weighting method to fuse the IMU signals and the plantar pressure distribution signals at the feature level and used it for the FOG detection task. The Feature-Fusion-Concat model with the direct concatenation of feature vectors performs significantly better than the two unimodal models, verifying that there is a complementary relationship between plantar pressure distribution information and inertial information. And that the fusion of the two makes the gait information for the FOG detection task more adequate so that the model performance is significantly improved.

The Feature-Fusion-Weighted model with the adaptive weighting of features outperforms the Feature-Fusion-Concat model with the direct concatenation of feature vectors. As mentioned earlier, since the two modalities, plantar pressure distribution suction signals and IMU signals, contribute differently to the FOG detection task, there is a redundant or complementary relationship between the two features; directly concatenating the feature vectors in series implies that each feature has the same weight, ignoring the existence of this redundant or complementary relationship. The Feature-Fusion-Weighted model performs better than the Feature-Fusion-Weighted model by adding weights to each feature (as shown in Fig. 16) and automatically learning the weight parameters in the neural network, this redundant or complementary relationship can be identified, which in turn improves the detection performance of the fusion model.

The onset of FOG is the process of gradual deterioration of gait pattern, and we carried out the work of FOG prediction based on this feature. The FIR was proposed based on the changing pattern of the FI before the freezing episode for automatic labeling of the pre-FOG category. This labeling method obtains higher quality data, a larger number of samples, and better model prediction performance compared to directly labeling fixed-time length data as pre-FOG categories before freezing episodes. The prediction effect of the pre-FOG events labeling method using fixed duration was affected by the pre-FOG duration. In general, the longer the pre-FOG duration, the worse the prediction effect. When the pre-FOG duration exceeds (equals to) 3.5 s, the prediction effect is no longer acceptable. It indicates that most of the FOG appearing signs do not exceed 3.5 s, and the use of the fixed-length marker method requires special attention to the pre-FOG duration, otherwise it is difficult to obtain better results. In addition, the best prediction results were obtained throughout the experimental results

Table 6
Number of samples after data set relabeling.

pre-FOG duration	1.5 s	2.5 s	3.5 s	4.5 s	5.5 s	FIR
Number of pre-FOG	1059	2700	4388	6050	7749	3657

Table 7
Prediction results of different pre-FOG labeling methods.

pre-FOG duration	TPR	TNR	PPV	NPV	Accuracy	F1-Score
1.5 s	0.756	0.831	0.817	0.773	0.794	0.786
2.5 s	0.663	0.822	0.789	0.709	0.743	0.721
3.5 s	0.545	0.809	0.741	0.640	0.678	0.628
4.5 s	0.567	0.792	0.698	0.604	0.636	0.569
5.5 s	0.438	0.672	0.672	0.583	0.612	0.530
FIR	0.629	0.885	0.846	0.705	0.757	0.722

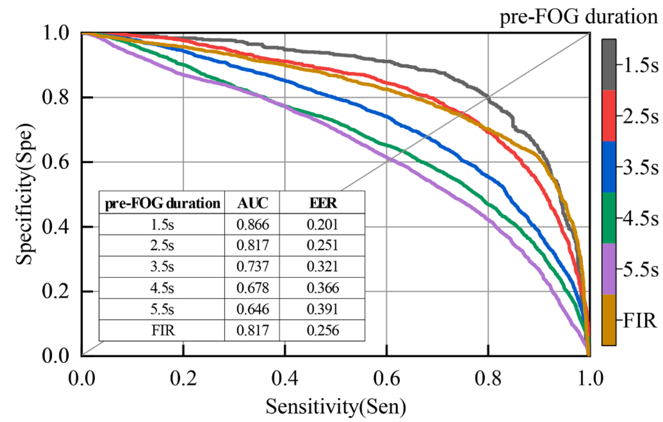

Fig. 15. ROC curves of the predicted results of different pre-FOG labeling methods.

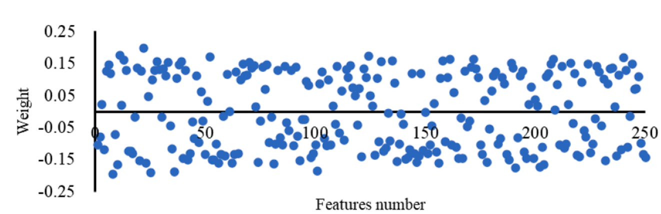

Fig. 16. Weight distribution of feature vectors after tandem.

when the pre-FOG duration was set to 1.5 s, with an F1 value of 0.786 and an AUC value of 0.866. The information on gait abnormalities contained in the data closer to the onset of FOG became more and more obvious, and, understandably, the best results for FOG prediction were obtained using only the 1.5 s segment of data before the onset of freezing. However, it should be noted that the small number of samples obtained using the pre-FOG labeling method with a fixed duration of 1.5 s is very unfavorable for conducting studies related to FOG prediction, which is the reason why we propose the FIR labeling method. When the pre-FOG duration was extended to 2.5 s, the prediction performance of the fixed-length tagging method was already lower than that of the FIR method, and the number of samples obtained was significantly less than that of the FIR method, indicating that some freezing signs with longer durations were not obtained by the 2.5-second fixed-length tagging method, and some of the pre-FOG category data obtained by the 2.5-second fixed-length tagging method were also of lower quality than that of the FIR method.

This pilot study has several limitations that need to be recognized. Firstly, all experiments were conducted in a medical room, which may lead to slight differences between the patient's gait and that of daily life. Secondly, Fig. 15 shows the weights assigned to each feature by the Feature-Fusion-Weighted model. The weights reflect the importance of the features, but we cannot yet provide clinical experts with the "interpretability" of these features, which requires a great deal of analytical work that we will carry out in subsequent studies. In addition, patients in different regions, age groups, and with different underlying diseases need to be added to the existing dataset to improve the robustness of the model.

5. Conclusion

Bächlin et al. [14] suggested in their study that sensor fusion might further improve the performance of FOG detection, so this paper proposed a new FOG detection method based on previous studies, which addresses the lack of gait kinematic information in the pure IMU signal, introduces the plantar pressure distribution signal, and fuses the two signals in a series of multimodal feature vectors to obtain a sensitivity of 0.911 and a specificity of 0.959. Compared with the unimodal model, the multimodal fusion-based FOG detection method improved the accuracy by 1.5 % with the same data set.

Since the features extracted from the plantar pressure distribution signal and the IMU signal do not contribute to the FOG detection to the same extent, an adaptive weighted feature fusion method was introduced to enhance the influence of important features on the detection results while weakening the influence of unimportant features on the detection results. The improved method has higher sensitivity, specificity, and accuracy compared to the direct cascade method.

In addition, FOG prediction work was conducted in this paper, and a method to automatically label pre-FOG categories by computing FIR was proposed. Compared with directly labeling the 2.5 s of data before the freezing episode as a pre-FOG event, this automatic labeling method obtained more samples and improved the prediction accuracy by 1.4 %, and at the same time, researchers no longer need to select the best labeling time period by trying different pre-FOG labeling times several times, and the labeling of pre-FOG for different patients depends entirely on their walking status, which will greatly reduce the workload of the investigators. In addition, this approach is more convincing for clinicians because it is determined based on the patient's walking status.

Finally, our detection and prediction methods can be well integrated into monitoring and intervention systems and hold great promise for long-term monitoring and telemedicine, which would certainly be very convenient for patients.

CRediT authorship contribution statement

Bochen Li: Data curation, Methodology, Software, Validation, Writing – original draft. **Yan Li:** Data curation, Writing – original draft. **Yining Sun:** Conceptualization, Resources, Supervision. **Xianjun Yang:** Conceptualization, Resources, Supervision. **Xu Zhou:** Investigation. **Zhiming Yao:** Project administration, Writing – review & editing.

Declaration of Competing Interest

The authors declare that they have no known competing financial interests or personal relationships that could have appeared to influence the work reported in this paper.

Data availability

The data that has been used is confidential.

Acknowledgment

We thank all subjects in this experiment. This work was supported by the Joint Research Fund for Chronic Disease Prevention and Control of Anhui Medical University and Institute of Intelligent Machines, CAS (grant No. MBLHJJ202004), Anhui Provincial Natural Science Foundation (grant No. 2108085MF232 and 1908085QH344), and Science and Technology Major Project of Anhui Province (grant No. 2020b05050002).

References

[1] A. Nieuwboer, W.D. Weerdt, R. Dom, E. Lesaffre, A frequency and correlation analysis of motor deficits in Parkinson patients, Disabil. Rehabil. 20 (4) (1998) 142–150.
[2] S.J.G. Lewis, J.M. Shine, The next step: a common neural mechanism for freezing of gait, Neuroscientist 22 (1) (2014) 72–82.
[3] W.-S. Zhang, C. Gao, Y.-Y. Tan, S.-D. Chen, Prevalence of freezing of gait in Parkinson's disease: a systematic review and meta-analysis, J. Neurol. 268 (11) (2021) 4138–4150.
[4] E.B. Forsaa, J.P. Larsen, T. Wentzel-Larsen, G. Alves, A 12-year population-based study of freezing of gait in Parkinson's disease, Parkinsonism Relat. Disord. 21 (3) (2015) 254–258.
[5] S. Perez-Lloret, et al., Prevalence, determinants, and effect on quality of life of freezing of gait in Parkinson disease, JAMA Neurol. 71 (7) (2014) 884–890.
[6] M.M. Hoehn, M.D. Yahr, Parkinsonism: onset, progression and mortality, Neurology 17 (5) (1967) 427–442 (in eng).
[7] S.T. Moore, H.G. MacDougall, W.G. Ondo, Ambulatory monitoring of freezing of gait in Parkinson's disease, J. Neurosci. Methods 167 (2) (2008) 340–348.
[8] Y.F. Chang, J.J. Ding, H. Hu, W.C. Yang, K.H. Lin, P.H. Wu, A real-time detection algorithm for freezing of gait in Parkinson's disease, in: 2014 IEEE International Symposium on Circuits and Systems (ISCAS), IEEE, 2014, pp. 1312–1315.
[9] M. Bächlin, J.M. Hausdorff, D. Roggen, N. Giladi, M. Plotnik, G. Tröster, Online detection of freezing of gait in Parkinson's disease patients: a performance characterization, in: Proceedings of the Fourth International Conference on Body Area Networks, Los Angeles, California, 2009, p. Article 11: ICST.
[10] C.A. Coste, B. Sijobert, R. Pissard-Gibollet, M. Pasquier, B. Espiau, C. Geny, Detection of freezing of gait in Parkinson disease: preliminary results, Sensors (Basel, Switzerland) 14 (4) (2014) 6819–6827 (in eng).
[11] S. Mazilu et al., Online detection of freezing of gait with smartphones and machine learning techniques, in: 2012 6th International Conference on Pervasive Computing Technologies for Healthcare (PervasiveHealth) and Workshops, 2012, pp. 123–130.
[12] L. Pepa, L. Ciabattoni, F. Verdini, M. Capecci, and M. Ceravolo, Smartphone based Fuzzy Logic freezing of gait detection in Parkinson's disease, 2014.
[13] A.S. Ashour, A. El-Attar, N. Dey, M.M.A. El-Naby, H.A. El-Kader, Patient-dependent freezing of gait detection using signals from multi-accelerometer sensors in Parkinson's disease, in: 2018 9th Cairo International Biomedical Engineering Conference (CIBEC), IEEE, 2018, pp. 171–174.
[14] M. Bächlin, et al., Wearable assistant for Parkinson's disease patients with the freezing of gait symptom, IEEE Trans. Inf Technol. Biomed. 14 (2) (2010) 436–446 (in eng).
[15] A. El-Attar, A.S. Ashour, N. Dey, H. Abdelkader, M.M. Abd El-Naby, R.S. Sherratt, Discrete wavelet transform-based freezing of gait detection in Parkinson's disease, J. Exp. Theor. Artif. Intell. 33 (4) (2021) 543–559 (in English).
[16] A. El-Attar, A.S. Ashour, N. Dey, H.A. El-Kader, M.M.A. El-Naby, F. Shi, Hybrid DWT-FFT features for detecting freezing of gait in Parkinson's disease, in: ITITS, 2018.
[17] A.S. Ashour, A. El-Attar, N. Dey, H. Abd El-Kader, M.M. Abd El-Naby, Long short term memory based patient-dependent model for FOG detection in Parkinson's disease, Pattern Recogn. Lett. 131 (2020) 23–29.

[18] B. Li, Z. Yao, J. Wang, S. Wang, X. Yang, Y. Sun, Improved deep learning technique to detect freezing of gait in Parkinson's disease based on wearable sensors, Electronics 9 (11) (2020).
[19] J. Howcroft, J. Kofman, E.D. Lemaire, Feature selection for elderly faller classification based on wearable sensors, J. Neuroeng. Rehabil. 14 (1) (2017) 47.
[20] G. Shalin, S. Pardoel, J. Nantel, E.D. Lemaire, J. Kofman, Prediction of freezing of gait in Parkinson's disease from foot plantar-pressure arrays using a convolutional neural network, in: 2020 42nd Annual International Conference of the IEEE Engineering in Medicine & Biology Society (EMBC), IEEE, 2020, pp. 244–247.
[21] R. Chee, A. Murphy, M. Danoudis, N. Georgiou-Karistianis, R. Iansek, Gait freezing in Parkinson's disease and the stride length sequence effect interaction, Brain 132 (Pt 8) (2009) 2151–2160 (in eng).
[22] R. Iansek, F. Huxham, J. McGinley, The sequence effect and gait festination in Parkinson disease: contributors to freezing of gait? Mov. Disord. 21 (9) (2006) 1419–1424.
[23] D.A. Yungher et al., Temporal characteristics of high-frequency lower-limb oscillation during freezing of gait in Parkinson's disease, Parkinson's Disease 2014 (2014) 606427.
[24] Z.-Q. Zhao, P. Zheng, S.-T. Xu, X. Wu, Object detection with deep learning: a review, IEEE Trans. Neural Netw. 30 (11) (2019) 3212–3232.
[25] F. Demrozi, R. Bacchin, S. Tamburin, M. Cristani, G. Pravadelli, Toward a wearable system for predicting freezing of gait in people affected by Parkinson's disease, IEEE J. Biomed. Health Inform. 24 (9) (2020) 2444–2451 (in eng).
[26] N. Naghavi, A. Miller, E. Wade, Towards real-time prediction of freezing of gait in patients with Parkinson's disease: addressing the class imbalance problem, Sensors 19 (18) (2019) 3898.
[27] V.G. Torvi, A. Bhattacharya, S. Chakraborty, Deep domain adaptation to predict freezing of gait in patients with Parkinson's disease, in: 2018 17th IEEE International Conference on Machine Learning and Applications (ICMLA), IEEE, 2018, pp. 1001–1006.
[28] Y. Zhang, W. Yan, Y. Yao, J.B. Ahmed, Y. Tan, D. Gu, Prediction of freezing of gait in patients with Parkinson's disease by identifying impaired gait patterns, IEEE Trans. Neural Syst. Rehabil. Eng. 28 (3) (2020) 591–600.
[29] C. Zhang, S. Pan, Y. Qi, Y. Yang, A footprint extraction and recognition algorithm based on plantar pressure, Traitement du Signal 36 (2019) 419–424.
[30] B. Li et al., Analysis of plantar pressure image based on flexible force-sensitive sensor array, in: Presented at the 2020 13th International Symposium on Computational Intelligence and Design (ISCID), 2020.
[31] K. Merry, M. MacPherson, E. Macdonald, M. Ryan, E.J. Park, C.J. Sparrey, Differentiating sitting, standing, and walking through regional plantar pressure characteristics, J. Biomech. Eng. 142 (4) (2020).
[32] S.J. Ellis, H. Stoecklein, J.C. Yu, G. Syrkin, H. Hillstrom, J.T. Deland, The accuracy of an automasking algorithm in plantar pressure measurements, Musculoskeletal J. Hosp. Spec. Surg. 7 (1) (2011) 57–63 (in eng).
[33] C.K. See, et al., Automated identification of diabetes type-2 subjects with and without neuropathy using eigenvalues, Proc. Inst. Mech. Eng. H 224 (1) (2010) 43–52.
[34] S. Ioffe, C. Szegedy, Batch normalization: accelerating deep network training by reducing internal covariate shift, in: Proceedings of the 32nd International Conference on International Conference on Machine Learning, Lille, France, 2015, pp. 448–456: JMLR.org.